Role of Precursors and Doping Agents in Producing 3D-Printed PEGDA–PDANI Electroactive Composites by an In Situ Polymerization Approach

The role of the precursors and dopant agents for producing 3D printed PEGDA-PDANI electroactive composites by an in-situ polymerization approach

*Rocco Carcione[a], Ignazio Roppolo[b], Annalisa Chiappone[c], Matteo Cocuzza[a,b,d], Simone Luigi Marasso [a,d], Emanuela Tamburri[e] and Silvia Battistoni[a]**

a Consiglio Nazionale delle Ricerche, Institute of Materials for Electronics and Magnetism (CNR-IMEM), Parco Area delle Scienze 37A, Parma, 43124 Italy

b Department of Applied Science and Technology, Politecnico Di Torino, Corso Duca Degli Abruzzi 24, 10129, Turin, Italy;

c Dipartimento di Scienze Chimiche e Geologiche, Università di Cagliari, S.S. 554 bivio Sestu, Monserrato, 09042, Italy

d Chilab—Materials and Microsystems Laboratory, DISAT, Politecnico di Torino, Corso Duca degli Abruzzi, 24, Chivasso (Turin), 10129 Italy

e Dip.to di Scienze e Tecnologie Chimiche & UdR INSTM di Roma - Università degli Studi di Roma "Tor Vergata" - Via della Ricerca Scientifica Rome 00133, Italy

KEYWORDS: Conductive polymers, additive manufacturing, electrically responsive 3D objects, in-situ polymerization, polyaniline.

ABSTRACT: The methodologies for producing composites materials based on conducting polymers (CPs) and 3D printed polymeric items are promising to combine the complex geometries of 3D objects with the charge transport properties of CPs. Among the latter, polyaniline (PANI) has an edge thanks to its peculiar electrochemical behavior. Synthesis protocols starting from the aniline monomer to produce PANI phase are consolidated, however a series of controversies is related to the use of this reactant, including potential toxicity. To obtain safer synthetic procedures for fabricating electrical and electrochemically active 3D composites materials, this research exploits an alternative precursor, namely the aniline dimer (DANI), for the in-situ synthesis of polydianiline (PDANI) via oxidative polymerization within 3D printed polyethylene glycol diacrylate (PEGDA) objects. Factors such as the molecular weight and swelling degree of PEGDA matrix, as well as the nature of the PDANI's dopant agents are found crucial to modulate the type of redox mechanism, the charge transport properties and the impedimetric response of 3D printed PEGDA-PDANI composites. The possibility to produce PEGDA objects in complex 3D shapes (discs, dumbbell and trabecular structures), coupled with the charge transport and electroactive performances of the PDANI filler, are promising for exploiting PEGDA-PDANI systems as active interfaces in a wide range of electronic applications.

INTRODUCTION

3D printing technologies, also branded as additive manufacturing (AM), have demonstrated a significant impact on a wide range of industries and fields, including product design, prototyping and production [1–4].

AM allows designers and engineers to create 3D objects with complex and customized shapes, increasing design flexibility and leading to the development of innovative products with enhanced functionalities [5–11]. Among the different 3D printing technologies, light induced ones (stereolithography – SL and Digital Light Processing – DLP) are well acknowledged for their superior precision and possibility to produce complex objects without the use of sacrificial materials [12].

Most 3D printable polymers are poor conductors of electricity, while many industrial, biomedical and research applications, ranging from biomedical devices to soft robotics[13], from stretchable electronics[6] to artificial muscles, from chemical sensors to transistors[9], from microelectromechanical systems to smart prosthetic devices[4], require electrical stimuli transmission. To overcome these limits, the scientific community is exploring materials [4], printing techniques [14] and post-processing methods to make the 3D printed objects electrically responsive[1]. For example, conductive inks based on the incorporation of conductive fillers within the polymeric matrix [6,15] were purposely formulated for specific 3D printing processes, such as direct ink writing [16]. Alternatively, a valid approach is to deposit electrically conductive coatings on the 3D printed objects surfaces. In this context, electrically conductive polymers (CPs) are largely used, since they allow to maintain the mechanical performances of the 3D substrates, while improving their electrical conductivity [17,18].

In addition, their use has the advantage to tailor the charge transport properties of the final objects by adjusting the composition of the polymer and the reaction conditions during the

synthesis process, along with cost effectiveness and versatility. The process of coating 3D printed items with CPs typically involves the application of a thin layer of the polymer onto the surface of the object, either by brushing, spraying, or dip-coating [19]. However, a more fascinating route consists in exploiting the *in-situ* polymerization of monomers or polymeric precursors to produce functional polymeric coatings, directly on the surface of the 3D objects [20,21]. Such an approach has the advantage to eliminate the need for isolating and purifying the polymer product, which simplifies the synthesis process and reduces the production costs [22–24]. Moreover, this strategy allows for the formation of the polymeric phase even within the host matrix, producing composite materials in which a continuous conductive network is formed both on the surface and within the whole 3D printed object. The monomers typically used for *in-situ* polymerization include aniline (ANI), 3,4-ethylenedioxythiophene (EDOT) and pyrrole to respectively produce polyaniline (PANI), poly(3,4-ethylenedioxythiophene) (PEDOT) and polypyrrole (PPy) [25,26]. In this scenario, PANI has an edge over the other CPs due to the combination of several properties, such as high synthesis yield by chemical oxidative polymerization, high electrical and ionic conductivities, high electrochemical activity, low cost for large-scale production and high stability in both air and water [27,28]. PANI films or composites have found large use in bioelectronics as main element in sensing, [27,29–31] memory [32,33] and so on devices [11,31,34]. In this view, the exploration of different deposition methods, 3D geometrical factors and innovative synthesis protocols may pave the way for the exploitation of PANI properties in several applications [11,15,26,35–37].

Although the synthetic protocols starting from the ANI monomer are consolidated and effective [7,29,38–40], a series of controversies is related to the use of this reagent, including a potential toxicity [41,42]. In order to obtain safer procedures, a key task of this research is to optimize the synthesis of PANI phase starting from the precursor N-phenyl-p-phenylenediamine (NPPD), also known as

dianiline (DANI). According to some studies, the involvement of such an aromatic diamine instead of ANI brings some typical advantages [41,43–46]. For example, DANI shows greater air and temperature stability [46,47] and is more soluble in polar solvents [43], thus resulting as a valid alternative for chemical reactions [46,47]. In this view, DANI is not only a handier reagent for processing operations, but also becomes a safer choice for a variety of applications, ranging from consumer goods to medical devices [42].

Despite the molecular structure of polydianiline (PDANI) is the same as that of PANI [48], few literature is reported on the synthesis protocols based on using DANI as a precursor [44,46,49–51]. The probable first synthesis of DANI oligomers can be traced back to 1930, when Yoffe et al. polymerized oligoaminodiphenylamines by the chemical oxidation of DANI with ferric chloride followed by reduction with phenylhydrazine [47]. More recently, Ćirić-Marjanović et al. investigated the PDANI synthesis via chemical oxidation of DANI with ammonium persulfate (APS) as oxidizing agent, focusing on the dependence on the APS:DANI molar ratio [47]. In the last years, Zhao et al. prepared PDANI materials by using different organic or inorganic acids as dopants, under the presence of cetyltrimethylammonium bromide (CTAB) as a structure-directing agent [44]. Anyway, to the best of our knowledge, *in-situ* polymerization protocols to produce electrically conductive and electrochemically active phases from DANI within 3D printed objects have never been settled yet.

In this context, the novelty of this research consists in the optimization of the PDANI synthesis starting from the DANI precursor, and the evaluation of the role and effects of several doping agents, such as HCl, H_2SO_4, (1S)-(+)-10-camphorsulfonic acids. The developed protocol has been adapted to an *in-situ* PDANI synthesis within the meshes of a polymer largely used in light-induced 3D printing, namely polyethylene glycol diacrylate (PEGDA), to produce electrically conductive

3D components [52]. Specifically, the polymer growth is obtained by means of a chemical oxidative polymerization of the DANI precursor by using APS as oxidant agent in acidic media for producing PDANI species in the emeraldine salt (ES) configuration, which is the electrically conductive form of the polymer. Scanning Electron Microscopy (SEM), Raman spectroscopy, Cyclic Voltammetry (CV) and Electrochemical Impedance Spectroscopy (EIS) analyses were performed for evaluating morphology, molecular structure and electroactivity of the samples. Factors such as PEGDA molecular weight and nature of the doping agents were taken into account to tune the performances of the produced 3D materials. In particular, the PEGDA swelling degree and the size of the dopant anions were found crucial parameters to tailor the type of redox mechanism, the charge transport properties and the impedimetric response of the composite objects.

Considering that the working principle of several organic electronic devices is based on the evolution of the redox signals [19,32], the possibility to produce PEGDA substrates in complex 3D shapes and geometries (discs, dumbbells, and trabecular structures), associated to the capability to provide specific electronic and electrochemical properties by CPs are promising aspects in the view of exploiting these hybrid systems as active interfaces in a wide range of electronic and electroanalytical applications. Moreover, the identification of non-toxic precursors, the use of environmentally friendly solvents and low quantity of reactants are desirable requisites for a more sustainable development of industrial, biomedical, and scientific research.

Overall, the *in-situ* growth of CPs within 3D printed objects provides a way to enhance the performance of the final product and simplify the manufacturing process, making it a promising approach for various applications in industries ranging from aerospace to medical devices and consumer goods.

MATERIALS AND METHODS

CHEMICALS

Aniline (ANI), ammonium persulphate (APS), sodium chloride (NaCl), dimethyl sulfoxide (DMSO), hydrochloric acid (HCl), sulfuric acid (H_2SO_4), (1S)-(+)-10-camphorsulfonic acid (CSA), ethanol, polyethylene glycol diacrylate (PEGDA) with three different molecular weights (namely, MW ~250, 575 and 700 Da) and phenylbis(2,4,6-trimethylbenzoyl)phosphine oxide (BAPO), used as photoinitiator, were purchased from Merck and used as received. N-phenyl-p-phenylenediamine (NPPD or DANI) was purchased by Alfa Aesar.

SYNTHESIS OF PDANI AND PANI SAMPLES

Reference and comparative PDANI and PANI samples were produced by means of chemical oxidative polymerization of DANI and ANI precursors, respectively, by using APS as oxidant agent. Equimolar amounts of reactants were allowed to react after an initial dispersion of the monomer in DMSO and the oxidant in 1 M HCl aqueous solution. Specifically, to promote the polymerization, APS/HCl solution was slowly dropped to the DANI/DMSO or ANI/DMSO solution kept at 0-5 °C by means of an ice bath. The syntheses lasted for 24 h, then the products were repetitively filtered and washed by water and ethanol to obtain dark green PDANI and PANI powders. Before the characterizations, the obtained samples were dried in air for 24 h. Table S1 lists the concentrations of the precursors and reagents used for the polymerization process.

3D PRINTING OF PEGDA SAMPLES

3D PEGDA supports were produced starting from photocurable formulations obtained by ultrasounds dispersion of 1%wt BAPO photoinitiator in three PEGDA batches at different MW, namely PEGDA-250, PEGDA-575 and PEGDA-700. The different STL files were prepared using

SolidWorks software. The printing process was performed by means of an Asiga (Alexandria, Australia) MAX X UV 27 DLP printer, equipped with a 385 nm LED light source. Irradiation times were 1.1 s, 1.5 s and 2 s for PEGDA-250, PEGDA-575 and PEGDA-700, respectively. Layer thickness was set at 100 μm, light intensity was fixed at 40 mW/cm^2. After printing, the samples were firstly soaked in an ethanol/water solution (50/50 v/v) to eliminate uncured resins, and then post cured for 5 min in a Robot Factory (Mirano, Italy) UV chamber equipped with a medium-pressure mercury lamp with light intensity of 12 mW/cm^2.

FABRICATION OF 3D PEGDA-PDANI AND PEGDA-PANI SAMPLES

The PEGDA-PDANI and reference PEGDA-PANI samples were produced according to a general protocol aimed at evaluating the effect of (i) the MW of the PEGDA matrix and (ii) the nature of the anionic dopant on the growth of the PDANI and PANI phases and their structural and functional properties.

(i) The different PEGDA samples, i.e., PEGDA-250, PEGDA-575 and PEGDA-700, were initially immersed for 24 h in DANI/DMSO or ANI/DMSO solutions for achieving an effective permeation of the starting monomer within the PEGDA matrix.

(ii) Subsequently, the APS oxidant was dissolved in the three different acidic media, i.e., 1 M HCl, 1 M H_2SO_4 and 1 M CSA, which were slowly dropped on the precursor impregnated PEGDA samples stored at 0-5 °C by means of an ice bath.

In this way *in-situ* polymerizations of DANI and ANI were promoted within the meshes of the PEGDA structures while maintaining the precursor/oxidant amount equimolar and varying the anionic dopant. The polymerization reactions lasted for 24 h, after that the products were repetitively washed by water and ethanol and gently dried in freezer at 0-4°C.

The names of samples along with the experimental parameters for the synthesis processes are reported in the Supporting Information. More in detail, Table S2 lists the produced 3D nanocomposites objects, along with the experimental parameters investigated to evaluate the effects of the insulating matrix; Table S3 reports names and synthesis conditions for the *in-situ* polymerization process within the 575 Da molecular weight PEGDA scaffolds to study the effects of the precursors; Table S4 lists the names and synthesis conditions for the production of 3D nanocomposite objects to assess the effects of the dopant agents.

CHARACTERIZATION TECHNIQUES

The samples' morphology was analyzed by means of an ultra-high-resolution Field Emission Scanning Electron Microscope (FESEM, Zeiss Supra 40, Carl Zeiss AG). Cross-section of the samples was obtained by cryofracturing the printed specimens in liquid nitrogen.

Raman spectra were collected in the range between 1000 and 1800 cm^{-1} by means of an Xplora ONE^{TM} (Horiba) instrument, under a laser source at 785 nm, 1% power, 100x magnification and 3 cm^{-1} spectral resolution with a grating set at 1200T. The Raman spectra were normalized and deconvolved by Lorentz function lines to derive position, amplitude, and integrated intensity for each peak.

The electrical conductivity was studied by performing *I-V* characteristics by using the four-probe technique. The probes were connected to a Keithley 6221 current source and a Keithley 2700 multimeter, controlled by LabVIEW interface. The electrical conductivity of the samples was calculated according to the procedure reported in Ref [53].

Electrochemical and impedimetric measurements were carried out in a standard one-compartment three-electrode cell by means of a Palm Sense compact electrochemical workstation. The produced samples acted as working electrode by using Pt foils as electrical contacts, a

saturated calomel electrode (SCE) and a Pt foil were used as reference and counter electrode, respectively. Cyclic voltammetry curves were collected in the (-0.2 ÷ +0.8) V potential range and at different scan-rates in 1 M HCl solution. EIS plots were acquired in 1 M HCl solution at frequencies varying from 1 Hz to 40 000 Hz, by applying a sinusoidal wave of 50 mV of amplitude superimposed to voltage bias ranging from 0 to +0.8 V. Fitting operation and data analysis were performed by using PSTrace software.

All the measurements were performed at room temperature (RT) on three replicas for each typology of sample.

RESULTS

The results of the preparation of PANI and PDANI samples are reported in Figure S1 and show that the DANI precursor does not alter the polyaniline structure as pointed out by SEM images, deconvolved Raman spectra and CV curves. Therefore, from a morphological, structural, and electrochemical perspective the substitution of ANI with DANI does not induce marked differences in the two final materials.

THE MOLECULAR WEIGHT AND THE SWELLING DEGREE OF PEGDA MATRIX

The general scheme adopted to grow PDANI and PANI phases within 3D PEGDA scaffolds by *in-situ* chemical oxidative polymerization routes is reported in Figure 1.

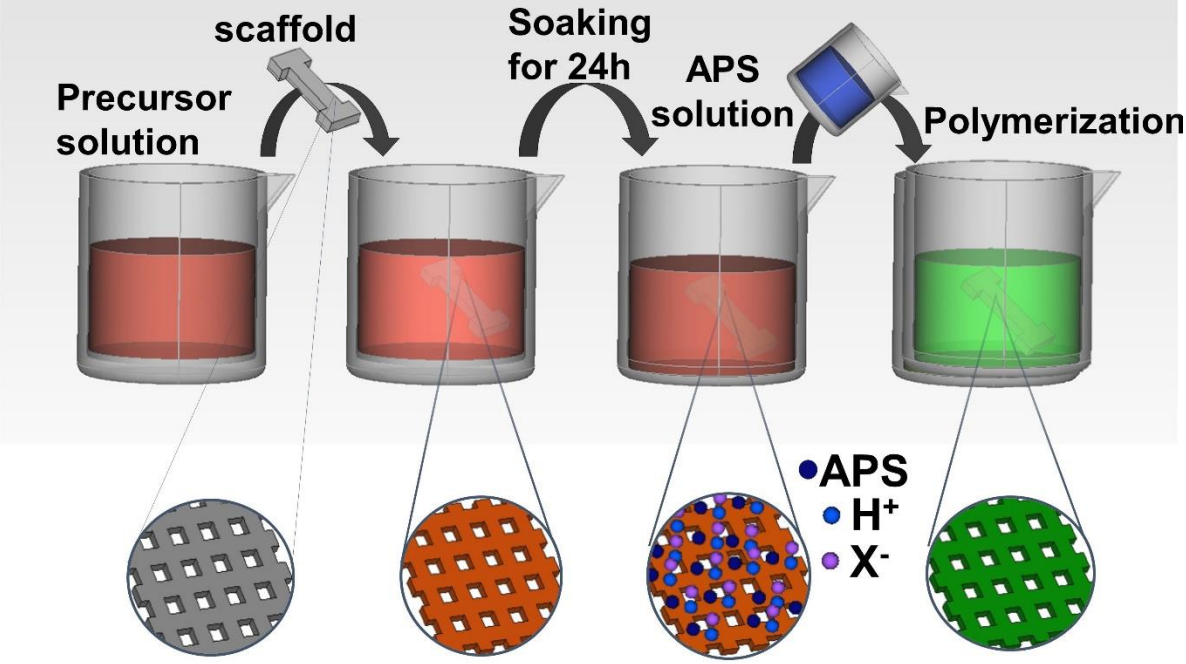

Figure 1: General scheme of the *in-situ* polymerization within PEGDA matrix via chemical oxidation methods. X- represents the dopant agent involved in the polymerization processes.

The permeation and adsorption of the precursors within the meshes of PEGDA scaffolds can be considered as pivotal steps to accomplish the *in-situ* polymerization processes. In fact, the adsorbed molecules are expected to behave as nucleation seeds for the following polymerization process. This issue was investigated by evaluating how the different PEGDA supports can influence the permeability to ANI and DANI molecules. It is well accepted that the molecular weight influences the crosslinking density (which decreases with MW increasing) and, in turns, the permeability or swelling of the final PEGDA hydrogel. The ANI and DANI polymerizations provided hybrid PEGDA-based composites with clearly different features. In Figure 2 are reported representative pictures showing the PP-250, PP-575 and PP-700 samples, produced by means of DANI polymerization within PEGDA-250, PEGDA-575 and PEGDA-700 substrates, respectively. For this set of experiments, the smallest dopant agent (i.e., Cl^- ion) was chosen to guarantee a homogeneous doping process, regardless the cross-linking density values.

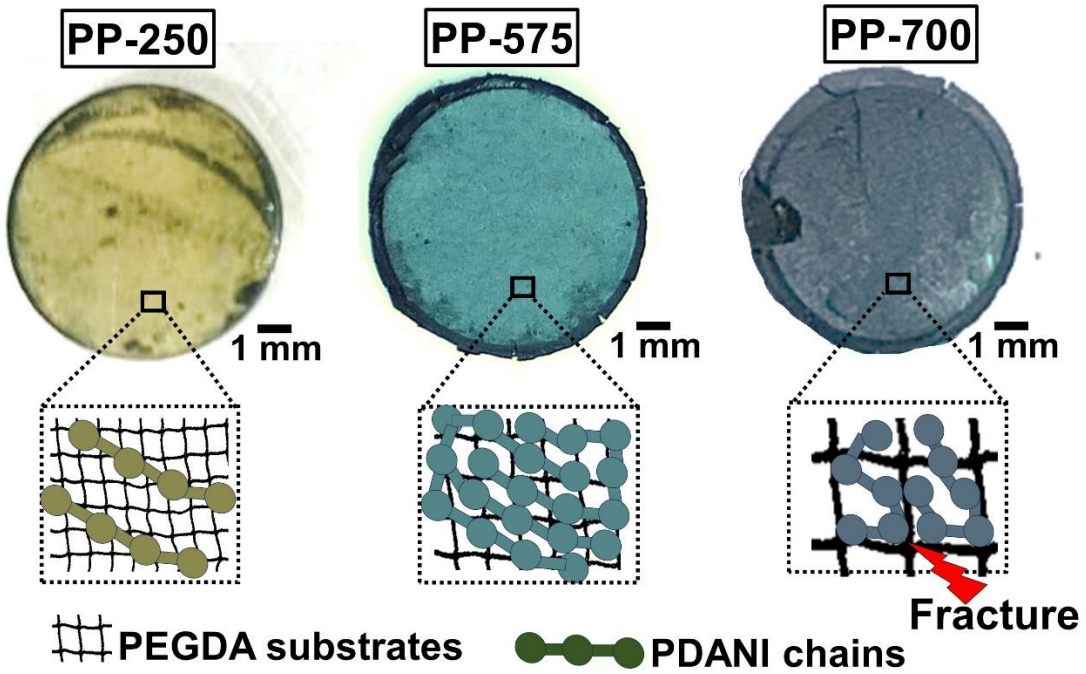

Figure 2: Pictures showing the PP-250, PP-575 and PP-700 samples with a disk geometry. Inset: Representation of the PDANI chains grown within the meshes of the PEGDA substrates.

We can observe that the PP-700 sample shows several cracks and exfoliations while the PP-250 and PP-575 samples are characterized by a rather widespread structural integrity. This outcome indicates that the low crosslinking density, associated with the highest MW, makes the PEGDA 700 support not suitable to work as hosting matrix, reasonably because the drying process leads to fractures and delamination. On the other hand, electrical measurements provided conductivity values on the order of 10^{-6} and 10^{-4} S $\cdot m^{-1}$ for PP-250 and PP-575 samples, respectively. The lower conductivity of PP-250 sample suggests that the high crosslinking density characterizing this substrate does not allow for a homogeneous distribution of both the starting monomer and the final conducting polymer within the PEGDA meshes, as schematically depicted in Figure 2. In view of the better mechanical and charge transport properties exhibited by the PEGDA-575-based composites, PEGDA-575 items were thus selected as substrates for further experiments.

THE EFFECT OF DIFFERENT MONOMERIC PRECURSOR

Figure 3 shows the results of a comparative study between two composite samples produced with the PEGDA-575 support and the two different ANI and DANI precursors. In particular, in Figure 3-a is reported a photo showing PEGDA-PANI and PEGDA-PDANI dumbbell shaped objects; Figure 3-b shows the respective Raman spectra; Figure 3-c and d illustrates the CV curves recorded at various scan rates in 1 M HCl medium by the two samples.

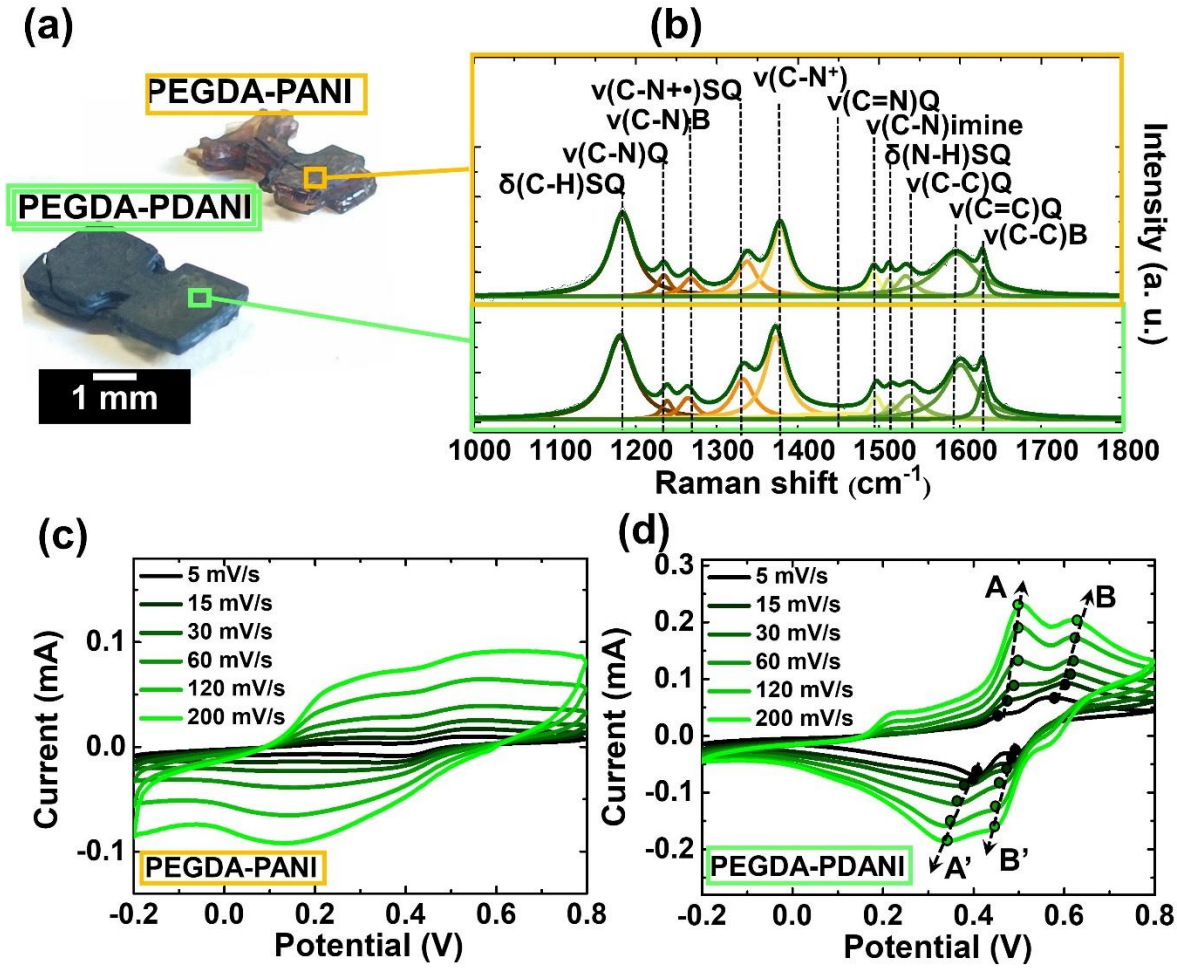

Figure 3: (a) Photo showing PEGDA-PANI and PEGDA-PDANI samples with a dumbbell geometry produced starting from PEGDA 575 supports: (b) representative deconvolved and normalized Raman spectra along with signals'

attribution and CV curves for (c) PEGDA-PANI and (d) PEGDA-PDANI samples at a scan rate varying from 5 to 200 mV/s in 1 M HCl solution.

The different coloring shown by the two composite samples (Figure 3-a) indicates that the synthesis of PDANI in PEGDA matrix took place in a much more homogeneous way than that of PANI. In fact, in the first case the formation of a uniformly colored emerald-green object was easily accomplished. This result can be explained by probable better interactions between the different starting monomers and PEGDA, which, in turn, were reasonably induced by their different solubility and reactivity in the reaction environment. The interactions between the PEGDA and PDANI phases reasonably occur between the polar groups along the polymeric backbones [54]. The Raman spectra of both the samples (Figure 3-b) indicate that the use of DANI precursor does not alter the PANI molecular structure, in perfect line with the result obtained for pure PDANI and PANI samples (Figure S1). In particular, the signals related to semiquinonoid (SQ) units indicate that both PANI or PDANI chains are mainly grown in the emeraldine salt (ES) configuration inside PEGDA meshes [38,55,56]. An in-depth analysis of the Raman spectra performed through the deconvolution operation allows for evaluating the protonation degree (PD%) of the main chains. In particular, the PD% was derived by the ratio between the integrated intensity of the peaks around 1320 cm^{-1} and 1255 cm^{-1}, respectively related to the protonated and deprotonated benzenoid units [57], by using Eq (1) [58]:

$$\boldsymbol{PD}\% = \frac{\boldsymbol{A_{1320}}}{\boldsymbol{A_{1225}+A_{1320}}}\boldsymbol{x\ 100} \qquad (1)$$

where A is the integrated area of the respective peaks. The similar PD% values of 85 and 81%, respectively found for PEGDA-PDANI and PEGDA-PANI samples, corroborate that the CPs produced within the PEGDA scaffolds possess comparable structural features.

The electroactivity was preliminarily evaluated by cyclic voltammetry measurements in 1 M HCl solution. As shown in Figure 3-c**,** the CV plots of PEGDA-PANI exhibit two broad oxidation peaks spread between +0.1 and +0.7 V and a single broad reduction signal at ca +0.15 V. Conversely, the CV curves of PEGDA-PDANI (Figure 3-d) show a scarcely detectable redox couple in the (+0.10 ÷ +0.20) V range, plausibly produced by the concomitant effect of hydrogen adsorption/desorption processes and the initial oxidation of the polymer chain [59,60] , and two clearly distinguishable redox couples, A-A' and B-B' signals, located in the (+0.50 ÷ +0.70) V potential range. The black dashed arrows depicted for these latter indicate the shift of the anodic and cathodic peaks towards greater and lower potentials, respectively, with the increasing of the sweep rate. Such a trend can be explained with the occurrence of redox processes under a diffusion regimen. Regarding the attribution of these signals, we can recall that polyaniline exists in different oxidation states, whose the more distinctive are the fully reduced leucoemeraldine (L), the semioxidized emeraldine (E), and the fully oxidized pernigraniline (P) form. In this view, the A-A' and B-B' redox pairs can be reasonably associated to the conversion among the different oxidation states of PANI, [31,61] as well as to the transformation between the intermediate p-benzoquinone and hydroquinone forms. [62–64] Anyhow, the comparison between the voltammograms of the two samples clearly points out that the electrochemistry of the polymer backbone is much more defined for PDANI than PANI based composite.

THE ROLE OF DIFFERENT DOPANT AGENTS

The evaluation of the dopant's role and the potential effects on the structural and function properties of the final products were investigated by focusing on PDANI phase. At the aim, a series of PEGDA-PDANI (PP) objects were fabricated by using Cl^-, SO_4^{2-} and CS^- as dopant agents for

producing PP-Cl, PP-SO_4 and PP-CS samples, respectively (Table S3). Photos, Raman spectra and a schematic representation of the doping processes are reported in Figure 4.

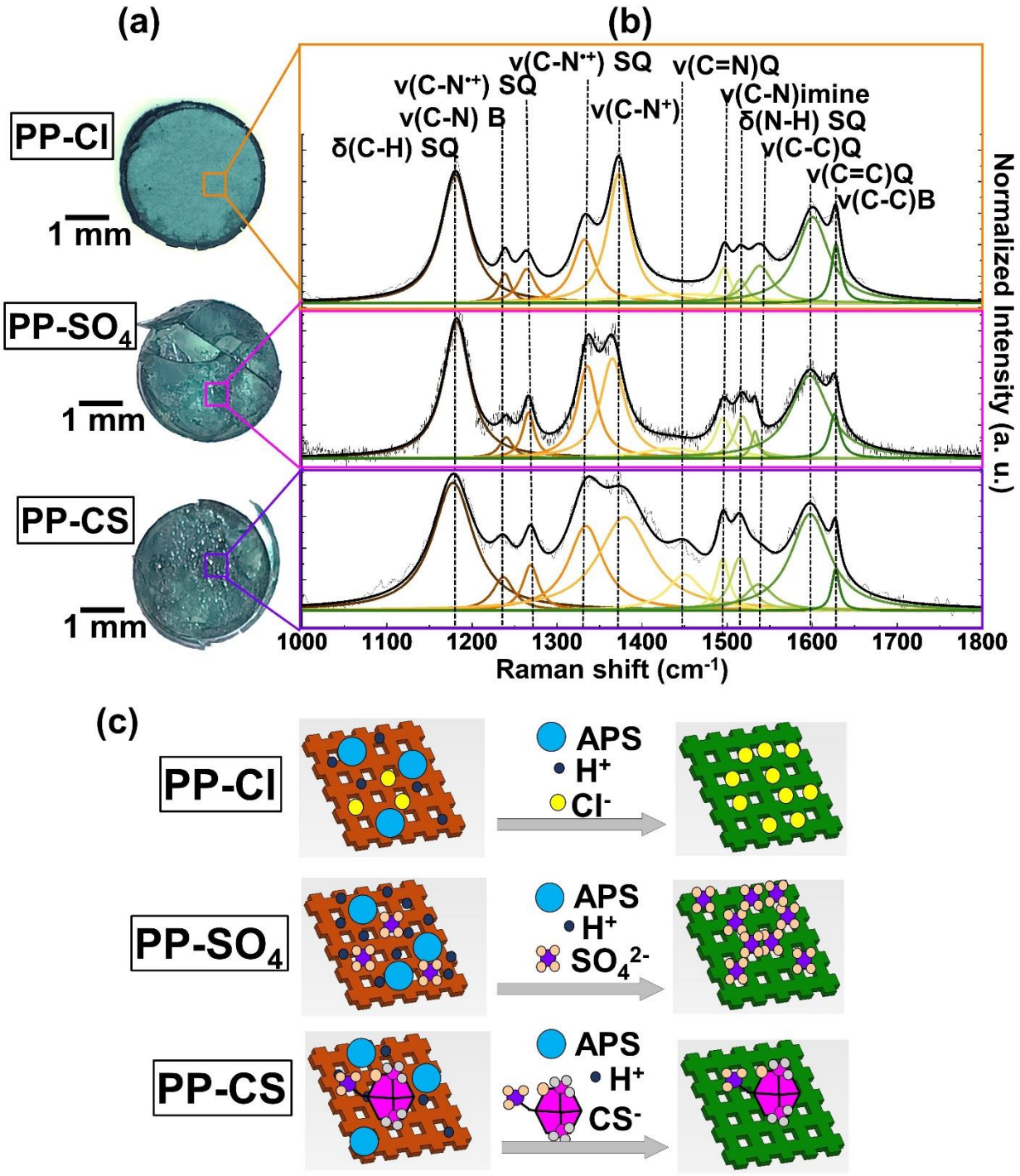

Figure 4: (a) Pictures showing PP-Cl, PP-SO_4 and PP-CS samples; (b) typical normalized and deconvolved Raman spectra along with peaks' attribution (c) schematic representation of the doping processes accomplished by different dopant agents.

As shown in Figure 4-a, the pictures indicate the maintenance of integrity of the pristine PEGDA substrates for PP-Cl and PP-CS samples. Conversely, cracks and exfoliations are observed for PP-SO_4 sample, which are probably due to the harsh environment of the 1 M H_2SO_4 solution. Although the acidic concentration was the same for all the PDANI syntheses, it is worthy to consider that the sulfuric acid is a strong dehydrating agent. Therefore, the involvement of this chemical species probably produces a degradation of the PEGDA chains.

The structural features of the PDANI phases were evaluated by means of Raman spectroscopy analysis. As shown in Figure 4-b, all the samples exhibit the signals typical of ES configuration. According to equation (1), a protonation grade (PD%) of 82, 89 and 78% was respectively derived for PP-Cl, PP-SO_4 and PP-CS, indicating that the dopant produces no substantial effects on the molecular structure of main chains. On the contrary, an electrical conductivity value of ~ 2.0×10^{-4}, 1.2×10^{-4} and lower than 1.0×10^{-5} $S \cdot m^{-1}$ was respectively derived for PP-Cl, PP-SO_4 and PP-CS. This result suggests that the incorporation of the big dopant CS^- anions within PDANI chains is somewhat sterically hampered by the PEGDA structure as graphically represented in Figure 4-c. Therefore, despite the remarkable protonation grade of PP-CS sample, a low doping level of the PDANI phase was plausibly obtained as to produce a PP-CS composite with moderate charge

transport properties. On the contrary, the small radius of the Cl^- and SO_4^{2-} anions are supposed to easily enter the hybrid PP matrices as to give slightly more conductive composite materials.

A study of the electroactivity of the PEGDA-PANI samples was carried out by means of CV measurements at various scan rates in 1 M HCl medium. CV curves, anodic peak current values as a function of the root scan rate and electrochemical stability test of the samples are reported in Figure 5.

As shown in Figure 5-a, the A-A' and B-B' redox couples are observed in all the voltammograms. In Figure 5-b the values of the anodic peak current (I_p^a) for the B-B' couple are

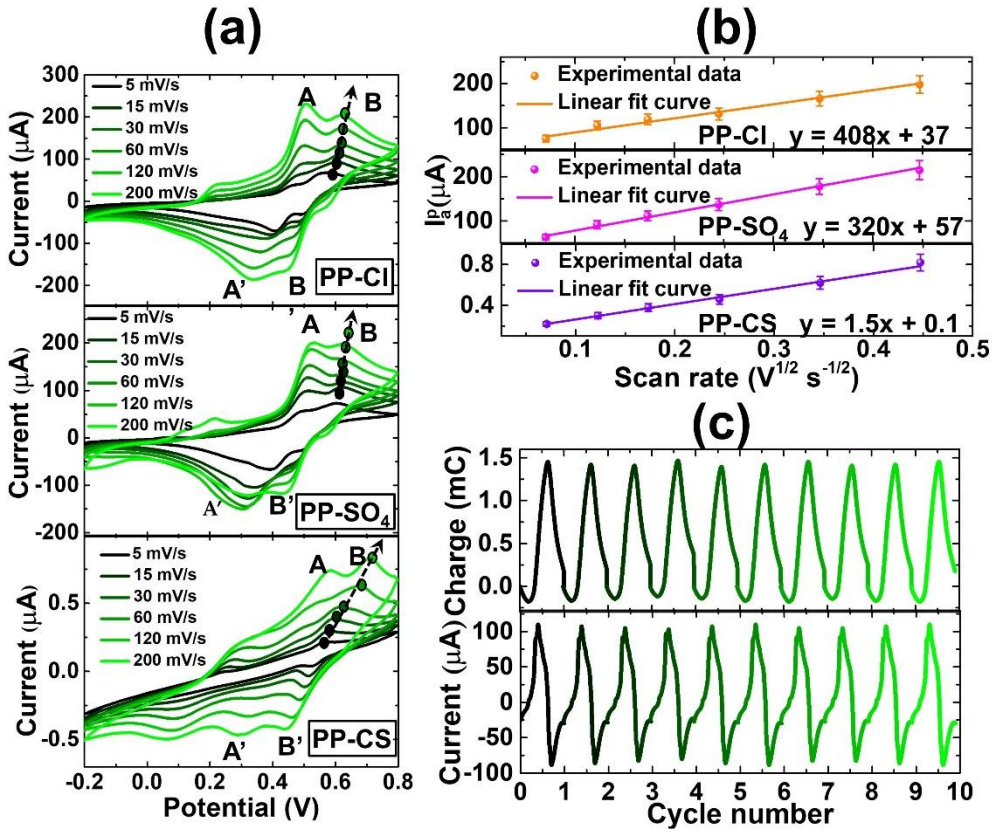

Figure 5: (a) CV curves at 5-15-30-60-120 and 200 mV/s in HCl 1M solution and (b) anodic peak current values as a function of the root scan rate for PP-Cl, PP-SO4 and PP-CS samples. The R^2 values derived by the fitting operation are 0.992, 0.966 and 0.994 for PP-Cl, PP-SO_4 and PP-CS samples, respectively. (c) Current and charge stability performances for PP-Cl samples at the scan rate of 30 mV/s in HCl 1M solution.

graphed as a function of the square root of the scan rate. The linear fitting of the experimental data indicates that the redox reactions producing these electrochemical signals occur under a diffusion regimen in all the samples. In line with the electrical characterization, the lower current values (~1 μA) are recorded for PP-CS, while similar current values approaching 250 μA are obtained for PP-Cl and PP-SO_4. These latter also show slopes which are two orders of magnitude higher than that of PP-CS. Finally, for all samples, the ratio between the absolute values of the anodic and cathodic peak currents is always greater than 1 at each scan rate. Taken together, all of these results suggest that the electrochemical processes emphasized by the voltammograms are generated by quasi-reversible reactions involving charge transfer processes of PDANI chains [65].

As it is well established in the literature, during an electrochemical event the structural changes, associated with the electron transfers from and onto the backbone of a CP, are typically accompanied by ion exchanges with the surrounding electrolytic solution for charge balancing. The mechanisms underlying these processes can involve anion or cation exchanges, and for PDANI phase they can be respectively described be the following Eqs. (2) and (3)[11,31]:

$$\mathrm{PDANI} + \mathrm{nA^-} + n\mathrm{H_2O} \rightleftharpoons (\mathrm{PDANI^{(n+)}}\mathrm{:}\ (\mathrm{A^-})_\mathrm{n}\mathrm{:}\ n\mathrm{H_2O}) + \mathrm{ne^-} \quad (2)$$

$$\mathrm{PDANI}\mathrm{:}\ (\mathrm{A^-})_\mathrm{n}\mathrm{:}\ (\mathrm{C^+})_\mathrm{n} \rightleftharpoons \mathrm{PDANI^{n+}}\mathrm{:}\ (\mathrm{A^-})_\mathrm{n} + \mathrm{ne^-} + \mathrm{n\,C^+} \quad (3)$$

The involvement of small size dopants, as in the case of Cl^- and SO_4^{2-} ions, is expected to drive the pathway based on anion exchange (Eq.2). According to this route, the oxidation reaction would encompass the insertion of anions, and a consequential swelling of the polymer matrix, whereas the reduction would be accomplished through the expulsion of anionic species and the subsequent shrinking of the polymer volume [66]. Conversely, the use of big size dopants, such as CS^- ions, would determine redox mechanisms based on cation exchange[67,68], where the opposite conformational modification is achieved by the expulsion and insertion of cations during oxidation and reduction processes, respectively (Eq.3). The collected CV measurements disclosed that the

doping process achieved by the incorporation of the big CS^- anions produces PDANI phases with rather modest electrochemical activity. In contrast, the PEGDA matrix does not significantly obstacles the incorporation and exchange of the small Cl^- and SO_4^{2-} ions, resulting in a best performing electrochemical behavior for both PP-Cl and PP-SO_4 composites. Finally, a last consideration can be made about the electrochemical stability curves reported in Figure 5-c. We can observe that for PP-Cl sample, both current and charge variations are rather stable over at least 10 cycles within the investigated voltage range of (-0.2 ÷0.8) V.

In the view of the overall results, we can reasonably assume that the chloride ion is the most effective dopant in producing a 3D PEGDA-CP based object in which there is the proper combination of structural, mechanical and charge transport properties exploitable for compelling applications.

Therefore, further electrochemical analyses were carried out only on the PP-Cl sample by means of in-depth EIS measurements.

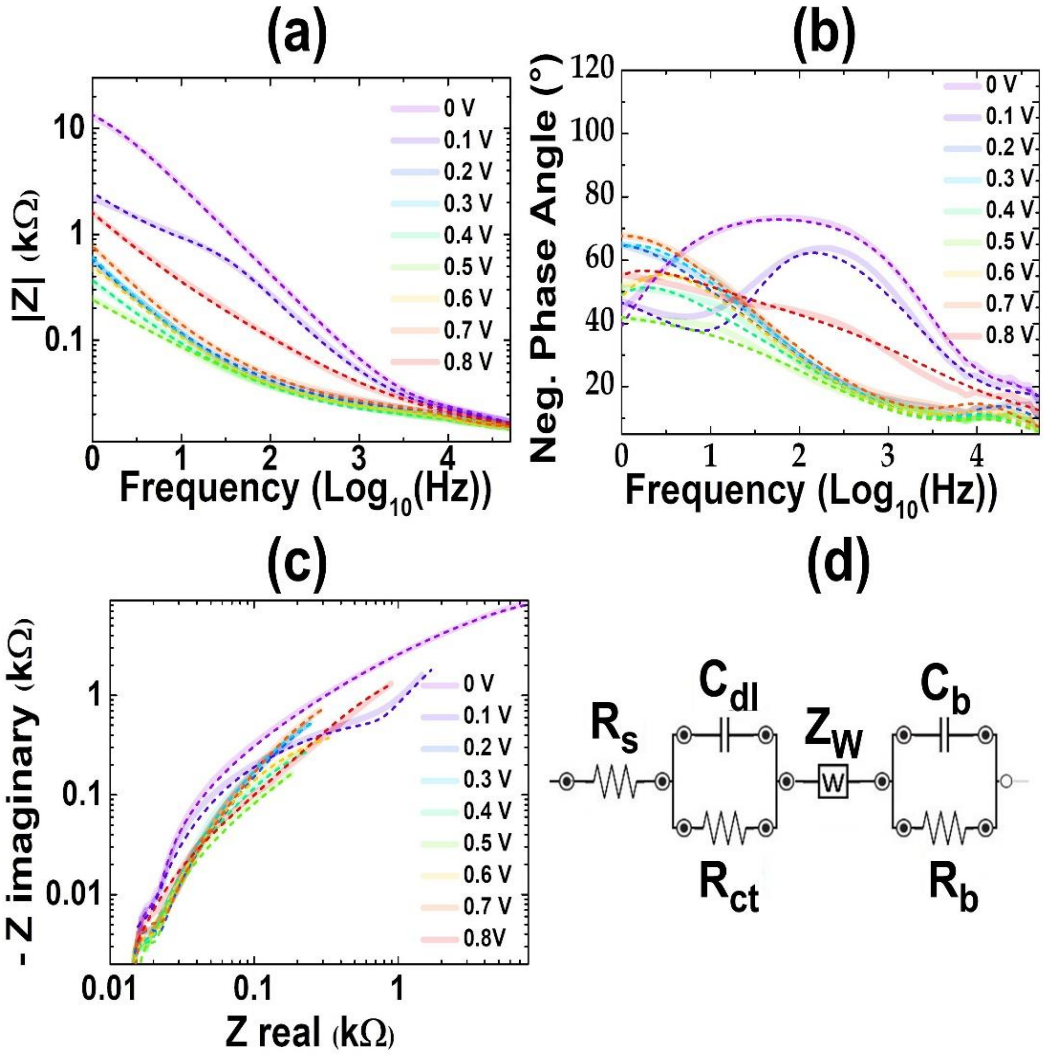

Figure 6: (a) Bode, (b) Nyquist and (c) negative phase angle EIS curves (straight lines) recorded for PP-Cl samples in 1 M HCl and relative fits (dotted lines); (d) equivalent electrical circuit to fit experimental data, where: R_s, is solution resistance, C_{dl} is the double layer capacitance at the electrode surface, R_{ct} is the charge transfer resistance), Z_W is the Warburg resistance, C_b and R_b are the bulk capacitance and resistance, respectively.

In Figure 6 are reported the EIS data recorded for PP-Cl samples in 1 M HCl at the applied bias of 0, 0.1, 0.2, 0.3, 0.4, 0.5, 0.6, 0.7 and 0.8 V, along with the simplest equivalent electrical circuit used for the fitting operation. The variation of the impedance spectra depending on the applied

voltage bias confirms once more the electroactivity of the sample. In particular, the spectra obtained at low bias (< 0.1 V) show the highest |Z| values, realistically due to the L form of the PDANI phase. With the bias increasing, the impedance absolute value progressively decreases up to reaching a minimum at 0.5 V. At this potential, the conversion to the E form can be considered completed. The further potential increase results in a parallel increase in |Z| attributable to the full oxidation of the PDANI chains. The easier circuit able to fit these redox transformations is reported in Figure 6-d where the R_s, C_{dl} and R_{ct} elements represent the electrolyte solution resistance, the double layer capacitance and the charge transfer resistance, respectively [69]. Different phenomena can contribute to the Warburg element (Z_W) such as surface inhomogeneities at electrode/electrolyte interface, hydrogen adsorption/desorption processes and dynamic disorder related with the anions' exchange between the solution and the composite bulk [69,70]. The C_b and R_b components can be instead related to the composite bulk capacitance and resistance, respectively [71].

Qualitative information on the magnitude and the trend of the different elements are reported in Table S5 and Figure S2, respectively. At each investigated potential, R_s varies only between 12 and 14 Ω values, indicating a low solution-composite interface resistance[72]. Analogously, C_b and R_b were found to vary in the 1-5 μF and 1-6 Ω small ranges, respectively. On the contrary, the bias application strongly tunes the values of the interface parameters, such as C_{dl}, R_{ct} and Z_W, disclosing that the interface properties are function of the oxidation states of PDANI chains. From the evolution of the fitting parameters with the applied bias, the conversion among the different oxidized forms of the PDANI phase is definitely confirmed (Figure S2). In fact, from an initial high value at 0 V, as the bias increases R_{ct} progressively decreases up to a minimum at 0.5 V following the fully conversion from L to E form. The further bias increase induces a 400% rise in

R_{ct} in line with the E to P conversion reaction. These hypotheses are well confirmed by the evolution of C_{dl}. According to the voltametric measurements (Figure 5), the significantly low value of C_{dl} at 0.5 V corroborate the occurrence of a faradic redox reaction. In contrast, an increase in C_{dl} value is recorded when non-faradic events take place. The overall electrochemical and interface properties changes of the PP-Cl system as a function of the oxidation state of PDANI chains convincingly point out that the PDANI filler can promote effective ion exchange with surroundings by transducing ionic current into electronic current via an efficient redox reaction [73]. In this view, the produced PP-Cl composite exhibits characteristics potentially exploitable in all those applications which require electrically and electrochemically active 3D materials.

To validate the efficiency of the proposed approach for producing objects with complex architectures, PEGDA items with sophisticated shapes were tested as substrates for *in-situ* polymerization of DANI.

In Figure 7 are shown photos of 3D printed PP-Cl samples with complex trabecular, dumbbell and cut disc geometries, along with low and high magnification cross-section SEM images showing the PEGDA multi-layered texture and the PDANI filler morphology.

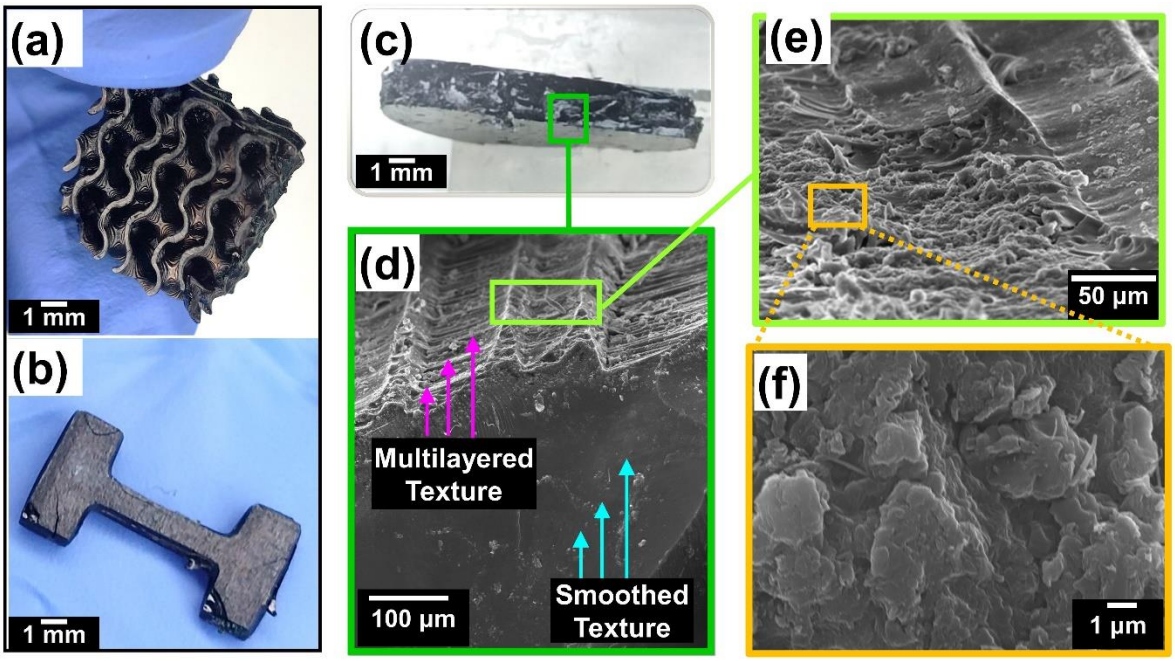

Figure 7: Pictures showing PP-Cl objects with (a) trabecular, (b) dumbbell and (c) a disk's cross section geometries; (d) high and (e-f) low magnification cross section SEM images for the PP-Cl samples to observe the multilayered texture of PEGDA objects and the morphology of PDANI fillers, respectively.

From the pictures (Figure 7-a, b) we can observe as the optimized protocol allows for successfully producing compact and homogeneous coloring and texture also for the printed objects with intricate trabecular and dumbbell shapes. The dark green coloration can be obviously related to the ES form of PDANI chains. The cross-section image of a cut PP-Cl disc (Figure 7-c) undoubtedly evidences that PDANI phase has uniformly grown within the PEGDA matrix, emphasizing that the proposed in-situ synthesis method permits the effective formation of a composite material. The cross section SEM image (Figure 7-d) highlights the multi-layered architecture of PEGDA-PDANI samples, given by the typical layer-by-layer deposition of 3D printing procedure[11]. Analogously, the smooth surface exhibited by this sample is in line with the high-quality surface finishing commonly achieved by means of light induced 3D printing technique [74]. Finally, a more in-depth observation of the morphology of sample cross-section

shows that actually PDANI globules are uniformly and densely distributed within the PEGDA matrix (Figure 7e-f).

CONCLUSIONS

The present research was focused on developing protocols for the *in-situ* oxidative polymerization of conjugated monomers within 3D printed PEGDA substrates to produce electrically conductive and electrochemically active PEGDA-based composites. Investigating ANI and DANI monomers as starting precursors, it was found that the synthesized PDANI filler gave PEGDA-PDANI objects with charge transport properties improved with respect to those of PEGDA-PANI ones.

The molecular weight of PEGDA matrix and the role of the PDANI chains' dopant were also studied as factors able to strongly modulate the properties of the final composite. The PEGDA system with medium molecular weight and swelling degree was identified as the proper substrate for growing PDANI phase with remarkable electrochemical activity, by maintaining at the same time the mechanical features of the pristine PEGDA support. Regarding the nature of the dopant agent, we pointed out that the use of small counterions of monoprotic acids, such as Cl^- ions, was decisive to guarantee reliable charge transfer and transport properties, impedimetric response, as well as structural integrity of the final material.

The possibility to produce PEGDA items with complex 3D shapes and geometries able to support the *in-situ* polymerization to give functional composites was finally checked.

The collected results can be considered a proof of principle for extending the proposed preparation protocol to a large-scale production of various 3D objects with sophisticated

architectures that could be effectively exploited in multiple applications, ranging from electronics to energy storage, as well as to biomedical devices.

ASSOCIATED CONTENT

Supporting Information. Samples' preparation; Synthesis of PDANI and PANI samples; Effects of the insulating matrix: PP-250, PP-575 and PP-700 samples; Effects of the precursor: PEGDA-PANI and PEGDA-PDANI samples; Effects of the dopant agent: PP(Cl), PP(SO4) and PP(CS) samples; SEM images, deconvolved Raman spectra and CV curves at 10

AUTHOR INFORMATION

Corresponding Author

* Corresponding author: silvia.battistoni@cnr.it

Author Contributions

Conceptualization, R.C. and S.B; investigation, R.C, I.R. and S.B; writing—original draft preparation, R.C., I.R., ET, S.B.; writing—review and editing, A.C., M.C., S.L.M. and E.T.; supervision, S.B and E.T.; project administration, S.B.; funding acquisition, S.B. All authors have read and agreed to the published version of the manuscript.

Funding Sources

This research was funded by the CNR project: "Hardware realization of reservoir computing and pattern recognition systems based on deterministic and stochastic organic memristive devices". Grant number B55F20002250005.

ACKNOWLEDGMENT

This research was funded by the CNR project: “Hardware realization of reservoir computing and pattern recognition systems based on deterministic and stochastic organic memristive devices”. Grant number B55F20002250005.

REFERENCES

(1) Park, S.; Shou, W.; Makatura, L.; Matusik, W.; Fu, K. (Kelvin). 3D Printing of Polymer Composites: Materials, Processes, and Applications. *Matter* **2022**, *5* (1), 43–76. https://doi.org/10.1016/j.matt.2021.10.018.

(2) Jandyal, A.; Chaturvedi, I.; Wazir, I.; Raina, A.; Ul Haq, M. I. 3D Printing – A Review of Processes, Materials and Applications in Industry 4.0. *Sustain. Oper. Comput.* **2022**, *3*. https://doi.org/10.1016/j.susoc.2021.09.004.

(3) Thakar, C. M.; Parkhe, S. S.; Jain, A.; Phasinam, K.; Murugesan, G.; Ventayen, R. J. M. 3d Printing: Basic Principles and Applications. In *Materials Today: Proceedings*; 2021; Vol. 51. https://doi.org/10.1016/j.matpr.2021.06.272.

(4) Arefin, A. M. E.; Khatri, N. R.; Kulkarni, N.; Egan, P. F. Polymer 3D Printing Review: Materials, Process, and Design Strategies for Medical Applications. *Polymers (Basel).* **2021**, *13* (9), 1499. https://doi.org/10.3390/polym13091499.

(5) Jordan, R. S.; Wang, Y. 3D Printing of Conjugated Polymers. *Journal of Polymer Science, Part B: Polymer Physics*. 2019. https://doi.org/10.1002/polb.24893.

(6) Yang, R.; Chen, X.; Zheng, Y.; Chen, K.; Zeng, W.; Wu, X. Recent Advances in the 3D Printing of Electrically Conductive Hydrogels for Flexible Electronics. *J. Mater. Chem. C* **2022**, *10* (14), 5380–5399. https://doi.org/10.1039/D1TC06162C.

(7) Politi, S.; Tamburri, E.; Carcione, R.; Lavecchia, T.; Angjellari, M.; Terranova, M. L. Innovative Preparation Processes and Structural Characteristics of 3D Printable Polymer-Based Nanocomposites. In *AIP Conference Proceedings*; 2019; Vol. 2196.

https://doi.org/10.1063/1.5140293.

(8) Angjellari, M.; Tamburri, E.; Montaina, L.; Natali, M.; Passeri, D.; Rossi, M.; Terranova, M. L. Beyond the Concepts of Nanocomposite and 3D Printing: PVA and Nanodiamonds for Layer-by-Layer Additive Manufacturing. *Mater. Des.* **2017**, *119*, 12–21. https://doi.org/10.1016/J.MATDES.2017.01.051.

(9) Scordo, G.; Bertana, V.; Ballesio, A.; Carcione, R.; Marasso, S. L.; Cocuzza, M.; Pirri, C. F.; Manachino, M.; Gomez, M. G.; Vitale, A.; Chiodoni, A.; Tamburri, E.; Scaltrito, L. Effect of Volatile Organic Compounds Adsorption on 3D-Printed Pegda:Pedot for Long-Term Monitoring Devices. *Nanomaterials* **2021**, *11* (1), 1–15. https://doi.org/10.3390/nano11010094.

(10) Ul Haq, A.; Montaina, L.; Pescosolido, F.; Carotenuto, F.; Trovalusci, F.; De Matteis, F.; Tamburri, E.; Di Nardo, P. Electrically Conductive Scaffolds Mimicking the Hierarchical Structure of Cardiac Myofibers. *Sci. Reports 2023 131* **2023**, *13* (1), 1–14. https://doi.org/10.1038/s41598-023-29780-w.

(11) Montaina, L.; Carcione, R.; Pescosolido, F.; Montalto, M.; Battistoni, S.; Tamburri, E. Three-Dimensional-Printed Polyethylene Glycol Diacrylate-Polyaniline Composites by In Situ Aniline Photopolymerization: An Innovative Biomaterial for Electrocardiogram Monitoring Systems. *ACS Appl. Electron. Mater.* **2023**, *5* (1), 164–172. https://doi.org/10.1021/acsaelm.2c01181.

(12) Gonzalez, G.; Roppolo, I.; Pirri, C. F.; Chiappone, A. Current and Emerging Trends in Polymeric 3D Printed Microfluidic Devices. *Addit. Manuf.* **2022**, *55*, 102867. https://doi.org/10.1016/J.ADDMA.2022.102867.

(13) Criado-Gonzalez, M.; Dominguez-Alfaro, A.; Lopez-Larrea, N.; Alegret, N.; Mecerreyes, D. Additive Manufacturing of Conducting Polymers: Recent Advances, Challenges, and Opportunities. *ACS Appl. Polym. Mater.* **2021**, *3* (6), 2865–2883. https://doi.org/10.1021/acsapm.1c00252.

(14) Bagheri, A.; Jin, J. Photopolymerization in 3D Printing. *ACS Appl. Polym. Mater.* **2019**, *1*

(4), 593–611. https://doi.org/10.1021/acsapm.8b00165.

(15) Yan, Y.; Jiang, Y.; Ng, E. L. L.; Zhang, Y.; Owh, C.; Wang, F.; Song, Q.; Feng, T.; Zhang, B.; Li, P.; Loh, X. J.; Chan, S. Y.; Chan, B. Q. Y. Progress and Opportunities in Additive Manufacturing of Electrically Conductive Polymer Composites. *Mater. Today Adv.* **2023**, *17*, 100333. https://doi.org/10.1016/j.mtadv.2022.100333.

(16) Yuk, H.; Lu, B.; Lin, S.; Qu, K.; Xu, J.; Luo, J.; Zhao, X. 3D Printing of Conducting Polymers. *Nat. Commun.* **2020**, *11* (1), 1604. https://doi.org/10.1038/s41467-020-15316-7.

(17) Wu, Y.; Chen, Y. X.; Yan, J.; Yang, S.; Dong, P.; Soman, P. Fabrication of Conductive Polyaniline Hydrogel Using Porogen Leaching and Projection Microstereolithography. *J. Mater. Chem. B* **2015**, *3* (26). https://doi.org/10.1039/c5tb00629e.

(18) Guarino, V.; Alvarez-Perez, M. A.; Borriello, A.; Napolitano, T.; Ambrosio, L. Conductive PANi/PEGDA Macroporous Hydrogels For Nerve Regeneration. *Adv. Healthc. Mater.* **2013**, *2* (1). https://doi.org/10.1002/adhm.201200152.

(19) Parmeggiani, M.; Ballesio, A.; Battistoni, S.; Carcione, R.; Cocuzza, M.; D'Angelo, P.; Erokhin, V. V.; Marasso, S. L.; Rinaldi, G.; Tarabella, G.; Vurro, D.; Pirri, C. F. Organic Bioelectronics Development in Italy: A Review. *Micromachines 2023, Vol. 14, Page 460* **2023**, *14* (2), 460. https://doi.org/10.3390/MI14020460.

(20) Wang, Y.; Liu, A.; Han, Y.; Li, T. Sensors Based on Conductive Polymers and Their Composites: A Review. *Polym. Int.* **2020**, *69* (1), 7–17. https://doi.org/10.1002/PI.5907.

(21) Nepomuceno, N. C.; Seixas, A. A. A.; Medeiros, E. S.; Mélo, T. J. A. Evaluation of Conductivity of Nanostructured Polyaniline/Cellulose Nanocrystals (PANI/CNC) Obtained via in Situ Polymerization. *J. Solid State Chem.* **2021**, *302*, 122372. https://doi.org/10.1016/J.JSSC.2021.122372.

(22) Zhao, Q.; Liu, X.; Stalin, S.; Khan, K.; Archer, L. A. Solid-State Polymer Electrolytes with in-Built Fast Interfacial Transport for Secondary Lithium Batteries. *Nat. Energy 2019 45* **2019**, *4* (5), 365–373. https://doi.org/10.1038/s41560-019-0349-7.

(23) Shen, Z.; Zhong, J.; Chen, J.; Xie, W.; Yang, K.; Lin, Y.; Chen, J.; Shi, Z. SiO2 Nanofiber Composite Gel Polymer Electrolyte by In-Situ Polymerization for Stable Li Metal Batteries. *Chinese Chem. Lett.* **2023**, *34* (3), 107370. https://doi.org/10.1016/J.CCLET.2022.03.093.

(24) Ma, L.; Chen, S.; Li, X.; Chen, A.; Dong, B.; Zhi, C. Liquid-Free All-Solid-State Zinc Batteries and Encapsulation-Free Flexible Batteries Enabled by In Situ Constructed Polymer Electrolyte. *Angew. Chemie* **2020**, *132* (52), 24044–24052. https://doi.org/10.1002/ANGE.202011788.

(25) Fantino, E.; Roppolo, I.; Zhang, D.; Xiao, J.; Chiappone, A.; Castellino, M.; Guo, Q.; Pirri, C. F.; Yang, J. 3D Printing/Interfacial Polymerization Coupling for the Fabrication of Conductive Hydrogel. *Macromol. Mater. Eng.* **2018**, *303* (4), 1700356. https://doi.org/10.1002/mame.201700356.

(26) Athukorala, S. S.; Tran, T. S.; Balu, R.; Truong, V. K.; Chapman, J.; Dutta, N. K.; Roy Choudhury, N. 3D Printable Electrically Conductive Hydrogel Scaffolds for Biomedical Applications: A Review. *Polymers (Basel).* **2021**, *13* (3), 474. https://doi.org/10.3390/polym13030474.

(27) Poddar, A. K.; Patel, S. S.; Patel, H. D. Synthesis, Characterization and Applications of Conductive Polymers: A Brief Review. *Polym. Adv. Technol.* **2021**, *32* (12), 4616–4641. https://doi.org/10.1002/PAT.5483.

(28) Du, X.; Xu, Y.; Xiong, L.; Bai, Y.; Zhu, J.; Mao, S. Polyaniline with High Crystallinity Degree: Synthesis, Structure, and Electrochemical Properties. *J. Appl. Polym. Sci* **2014**, 40827. https://doi.org/10.1002/app.40827.

(29) Li, Y.; Mao, Y.; Xiao, C.; Xu, X.; Li, X. Flexible PH Sensor Based on a Conductive PANI Membrane for PH Monitoring. *RSC Adv.* **2019**, *10* (1), 21–28. https://doi.org/10.1039/C9RA09188B.

(30) Hou, X.; Zhou, Y.; Liu, Y.; Wang, L.; Wang, J. Coaxial Electrospun Flexible PANI//PU Fibers as Highly Sensitive PH Wearable Sensor. *J. Mater. Sci.* **2020**, *55* (33), 16033–16047. https://doi.org/10.1007/s10853-020-05110-7.

(31) Politi, S.; Battistoni, S.; Carcione, R.; Montaina, L.; Macis, S.; Lupi, S.; Tamburri, E. PANI-Modified Ti-Doped CVD Diamond As Promising Conductive Platform to Mimic Bioelectricity Functions. *Adv. Mater. Interfaces* **2021**, *8* (24), 2101401. https://doi.org/10.1002/ADMI.202101401.

(32) Battistoni, S.; Cocuzza, M.; Marasso, S. L.; Verna, A.; Erokhin, V. The Role of the Internal Capacitance in Organic Memristive Device for Neuromorphic and Sensing Applications. *Adv. Electron. Mater.* **2021**, *7* (11), 2100494. https://doi.org/10.1002/aelm.202100494.

(33) Battistoni, S.; Erokhin, V.; Iannotta, S. Emulation with Organic Memristive Devices of Impairment of LTP Mechanism in Neurodegenerative Disease Pathology. *Neural Plast.* **2017**, *2017*, 1–8. https://doi.org/10.1155/2017/6090312.

(34) Battistoni, S.; Erokhin, V.; Iannotta, S. Frequency Driven Organic Memristive Devices for Neuromorphic Short Term and Long Term Plasticity. *Org. Electron.* **2019**, *65*, 434–438. https://doi.org/10.1016/j.orgel.2018.11.033.

(35) Alegret, N.; Dominguez-Alfaro, A.; Mecerreyes, D. 3D Scaffolds Based on Conductive Polymers for Biomedical Applications. *Biomacromolecules* **2019**, *20* (1), 73–89. https://doi.org/10.1021/acs.biomac.8b01382.

(36) Malakhova, Y. N.; Korovin, A. N.; Lapkin, D. A.; Malakhov, S. N.; Shcherban, V. V.; Pichkur, E. B.; Yakunin, S. N.; Demin, V. A.; Chvalun, S. N.; Erokhin, V. Planar and 3D Fibrous Polyaniline-Based Materials for Memristive Elements. *Soft Matter* **2017**, *13* (40), 7300–7306. https://doi.org/10.1039/C7SM01773A.

(37) Joo, H.; Cho, S. Comparative Studies on Polyurethane Composites Filled with Polyaniline and Graphene for DLP-Type 3D Printing. *Polymers (Basel).* **2020**, *12* (1). https://doi.org/10.3390/polym12010067.

(38) Tamburri, E.; Guglielmotti, V.; Orlanducci, S.; Terranova, M. L.; Sordi, D.; Passeri, D.; Matassa, R.; Rossi, M. Nanodiamond-Mediated Crystallization in Fibers of PANI Nanocomposites Produced by Template-Free Polymerization: Conductive and Thermal Properties of the Fibrillar Networks. *Polymer (Guildf).* **2012**, *53* (19), 4045–4053.

https://doi.org/10.1016/J.POLYMER.2012.07.014.

(39) Balint, R.; Cassidy, N. J.; Cartmell, S. H. Conductive Polymers: Towards a Smart Biomaterial for Tissue Engineering. *Acta Biomater.* **2014**, *10* (6), 2341–2353. https://doi.org/10.1016/J.ACTBIO.2014.02.015.

(40) Palmieri, E.; Montaina, L.; Polino, G.; Bonomo, M.; Giordanengo, G.; Barolo, C.; Paradossi, G.; Brunetti, F.; Tamburri, E.; Orlanducci, S. Engineered Surface for High Performance Electrodes on Paper. *Appl. Surf. Sci.* **2023**, *608*, 155117. https://doi.org/10.1016/J.APSUSC.2022.155117.

(41) Ranjith Kumar, D.; Dhakal, G.; Muhammed Shafi, P.; Saad Sayed, M.; Lee, J.; Lee, Y. R.; Shim, J. J. Sulfite Food Additive Electrochemical Determination by Nucleophilic Addition on Poly(4-Aminodiphenylamine)-4-Aminothiophenol-Au Composite Electrode. *Microchem. J.* **2022**, *181* (Di). https://doi.org/10.1016/j.microc.2022.107635.

(42) Giacobbe, S.; Pezzella, C.; Della Ventura, B.; Giacobelli, V. G.; Rossi, M.; Fontanarosa, C.; Amoresano, A.; Sannia, G.; Velotta, R.; Piscitelli, A. Green Synthesis of Conductive Polyaniline by Trametes Versicolor Laccase Using a DNA Template. *Eng. Life Sci.* **2019**, *19* (9), 631–642. https://doi.org/10.1002/elsc.201900078.

(43) Li, X.-G.; Huang, M.-R.; Duan, W.; Yang, Y.-L. Novel Multifunctional Polymers from Aromatic Diamines by Oxidative Polymerizations. *Chem. Rev.* **2002**, *102* (9), 2925–3030. https://doi.org/10.1021/cr010423z.

(44) Zhao, R.; Peng, H.; Wang, F.; Zhen, J.; Li, L.; Ma, G.; Lei, Z. Regulating the Species and the Counter-Ion Size of Proton Acids to Prepare Novel Poly(4-Aminodiphenylamine) Nanomaterials for Supercapacitors. *Mater. Chem. Front.* **2021**, *5* (16), 6145–6151. https://doi.org/10.1039/d1qm00690h.

(45) Lin, C. W.; Mak, W. H.; Chen, D.; Wang, H.; Aguilar, S.; Kaner, R. B. Catalytic Effects of Aniline Polymerization Assisted by Oligomers. *ACS Catal.* **2019**, *9* (8), 6596–6606. https://doi.org/10.1021/acscatal.9b01484.

(46) Peng, H.; Zhao, R.; Liang, J.; Wang, S.; Wang, F.; Zhou, J.; Ma, G.; Lei, Z. Template-

Confined Growth of Poly(4-Aminodiphenylamine) Nanosheets as Positive Electrode toward Superlong-Life Asymmetric Supercapacitor. *ACS Appl. Mater. Interfaces* **2018**, *10* (43), 37125–37134. https://doi.org/10.1021/acsami.8b14138.

(47) Ćirić-Marjanović, G.; Trchová, M.; Konyushenko, E. N.; Holler, P.; Stejskal, J. Chemical Oxidative Polymerization of Aminodiphenylamines. *J. Phys. Chem. B* **2008**, *112* (23), 6976–6987. https://doi.org/10.1021/jp710963e.

(48) Junker, K.; Luginbühl, S.; Schüttel, M.; Bertschi, L.; Kissner, R.; Schuler, L. D.; Rakvin, B.; Walde, P. Efficient Polymerization of the Aniline Dimer p -Aminodiphenylamine (PADPA) with Trametes Versicolor Laccase/O 2 as Catalyst and Oxidant and AOT Vesicles as Templates. *ACS Catal.* **2014**, *4* (10), 3421–3434. https://doi.org/10.1021/cs500769d.

(49) Bocchini, S.; Chiolerio, A.; Porro, S.; Accardo, D.; Garino, N.; Bejtka, K.; Perrone, D.; Pirri, C. F. Synthesis of Polyaniline-Based Inks, Doping Thereof and Test Device Printing towards Electronic Applications. *J. Mater. Chem. C* **2013**, *1* (33), 5101–5109. https://doi.org/10.1039/C3TC30764F.

(50) Chiolerio, A.; Bocchini, S.; Scaravaggi, F.; Porro, S.; Perrone, D.; Beretta, D.; Caironi, M.; Fabrizio Pirri, C. Synthesis of Polyaniline-Based Inks for Inkjet Printed Devices: Electrical Characterization Highlighting the Effect of Primary and Secondary Doping. *Semicond. Sci. Technol.* **2015**, *30* (10), 104001. https://doi.org/10.1088/0268-1242/30/10/104001.

(51) Chiolerio, A.; Bocchini, S.; Porro, S. Inkjet Printed Negative Supercapacitors: Synthesis of Polyaniline-Based Inks, Doping Agent Effect, and Advanced Electronic Devices Applications. *Adv. Funct. Mater.* **2014**, *24* (22), 3375–3383. https://doi.org/10.1002/adfm.201303371.

(52) Salas, A.; Zanatta, M.; Sans, V.; Roppolo, I. Chemistry in Light-Induced 3D Printing. *ChemTexts 2023 91* **2023**, *9* (1), 1–16. https://doi.org/10.1007/S40828-022-00176-Z.

(53) Smits, F. M. Measurement of Sheet Resistivities with the Four-Point Probe. *Bell Syst. Tech. J.* **1958**, *37* (3). https://doi.org/10.1002/j.1538-7305.1958.tb03883.x.

(54) Carcione, R.; Pescosolido, F.; Montaina, L.; Toschi, F.; Orlanducci, S.; Tamburri, E.;

Battistoni, S. Self-Standing 3D-Printed PEGDA–PANIs Electroconductive Hydrogel Composites for PH Monitoring. *Gels* **2023**, *9* (10), 784. https://doi.org/10.3390/gels9100784.

(55) Suendo, V.; Lau, Y.; Hidayat, F.; Reza, M.; Qadafi, A.; Rochliadi, A. Effect of Face-to-Face and Side-to-Side Interchain Interactions on the Electron Transport in Emeraldine Salt Polyaniline. *Phys. Chem. Chem. Phys.* **2021**, *23* (12), 7190–7199. https://doi.org/10.1039/d0cp06194h.

(56) Lindfors, T.; Ivaska, A. Raman Based PH Measurements with Polyaniline. *J. Electroanal. Chem.* **2005**, *580* (2), 320–329. https://doi.org/10.1016/j.jelechem.2005.03.042.

(57) Stejskal, J.; Trchová, M.; Bober, P.; Humpolíček, P.; Kašpárková, V.; Sapurina, I.; Shishov, M. A.; Varga, M. *Conducting Polymers: Polyaniline*; 2015. https://doi.org/10.1002/0471440264.pst640.

(58) Pescosolido, F.; Montaina, L.; Carcione, R.; Politi, S.; Matassa, R.; Carotenuto, F.; Nottola, S. A.; Nardo, P. Di; Tamburri, E. A New Strong-Acid Free Route to Produce Xanthan Gum-PANI Composite Scaffold Supporting Bioelectricity. *Macromol. Biosci.* **2023**, *7*, 2300132. https://doi.org/10.1002/mabi.202300132.

(59) Biabangard, F.; Nazari, H.; Arefinia, R. Effect of PH on the Electrochemical Properties of Polyaniline Nanoparticle Suspension in Strongly Acidic Solution: An Experimental and Theoretical Study. *J. Solid State Electrochem.* **2021**, *25* (3), 881–893. https://doi.org/10.1007/s10008-020-04863-0.

(60) Yan, B.; Yang, J.; Li, Y.; Cao, Y. Electrochemical Adsorption of Hydrogen and Various Ions on Polyaniline Film. Reactions Concerning the First Pair of Cyclic Voltammetric Peaks. *Synth. Met.* **1991**, *44* (2), 189–197. https://doi.org/10.1016/0379-6779(91)91834-W.

(61) Jamadade, V. S.; Dhawale, D. S.; Lokhande, C. D. Studies on Electrosynthesized Leucoemeraldine, Emeraldine and Pernigraniline Forms of Polyaniline Films and Their Supercapacitive Behavior. *Synth. Met.* **2010**, *160* (9–10), 955–960. https://doi.org/10.1016/j.synthmet.2010.02.007.

(62) Popov, A.; Brasiunas, B.; Mikoliunaite, L.; Bagdziunas, G.; Ramanavicius, A.; Ramanaviciene, A. Comparative Study of Polyaniline (PANI), Poly(3,4-Ethylenedioxythiophene) (PEDOT) and PANI-PEDOT Films Electrochemically Deposited on Transparent Indium Thin Oxide Based Electrodes. *Polymer (Guildf).* **2019**, *172*, 133–141. https://doi.org/10.1016/J.POLYMER.2019.03.059.

(63) Chen, W. C.; Wen, T. C.; Hu, C. C.; Gopalan, A. Identification of Inductive Behavior for Polyaniline via Electrochemical Impedance Spectroscopy. *Electrochim. Acta* **2002**, *47* (8), 1305–1315. https://doi.org/10.1016/S0013-4686(01)00849-0.

(64) Kuzmany, H.; Sariciftci, N. S. In Situ Spectro-Electrochemical Studies of Polyaniline. *Synth. Met.* **1987**, *18* (1–3), 353–358. https://doi.org/10.1016/0379-6779(87)90904-0.

(65) Effati, E.; Heidari, H.; Pourabbas, B. Synthesis of PEDOT in a Continuous Microfluidic System. *J. Polym. Res.* **2020**, *27* (9), 248. https://doi.org/10.1007/s10965-020-02205-2.

(66) Otero, T. F. Artificial Muscles Driven by the Cooperative Actuation of Electrochemical Molecular Machines. Persistent Discrepancies and Challenges. *Int. J. Smart Nano Mater.* **2017**, *8* (4), 125–143. https://doi.org/10.1080/19475411.2018.1434256.

(67) Beaumont, S.; Otero, T. F. The Response of Polypyrrole–DBS Electrochemical Molecular Motors to Na Concentration: Analogies in Cell Biology. *Electrochem. commun.* **2019**, *103*, 114–119. https://doi.org/10.1016/J.ELECOM.2019.05.011.

(68) Lyutov, V.; Tsakova, V. Polysulfonate-Doped Polyanilines—Oxidation of Ascorbic Acid and Dopamine in Neutral Solution. *J. Solid State Electrochem.* **2020**, *24* (11–12), 3113–3123. https://doi.org/10.1007/s10008-020-04771-3.

(69) Arabzadeh, H.; Shahidi, M.; Foroughi, M. M. Electrodeposited Polypyrrole Coatings on Mild Steel: Modeling the EIS Data with a New Equivalent Circuit and the Influence of Scan Rate and Cycle Number on the Corrosion Protection. *J. Electroanal. Chem.* **2017**, *807*, 162–173. https://doi.org/10.1016/J.JELECHEM.2017.11.019.

(70) Dubal, D. P.; Lee, S. H.; Kim, J. G.; Kim, W. B.; Lokhande, C. D. Porous Polypyrrole Clusters Prepared by Electropolymerization for a High Performance Supercapacitor. *J.*

Mater. Chem. **2012**, *22* (7), 3044–3052. https://doi.org/10.1039/C2JM14470K.

(71) Nuramdhani, I.; Gokceoren, A. T.; Odhiambo, S. A.; De Mey, G. D.; Hertleer, C.; Langenhove, L. Van. Electrochemical Impedance Analysis of a PEDOT:PSS-Based Textile Energy Storage Device. *Mater. 2018, Vol. 11, Page 48* **2017**, *11* (1), 48. https://doi.org/10.3390/MA11010048.

(72) Hallik, A.; Alumaa, A.; Tamm, J.; Sammelselg, V.; Väärtnõu, M.; Jänes, A.; Lust, E. Analysis of Electrochemical Impedance of Polypyrrole|sulfate and Polypyrrole|perchlorate Films. *Synth. Met.* **2006**, *156* (5–6), 488–494. https://doi.org/10.1016/J.SYNTHMET.2006.02.004.

(73) Samukaite-Bubniene, U.; Valiūnienė, A.; Bucinskas, V.; Genys, P.; Ratautaite, V.; Ramanaviciene, A.; Aksun, E.; Tereshchenko, A.; Zeybek, B.; Ramanavicius, A. Towards Supercapacitors: Cyclic Voltammetry and Fast Fourier Transform Electrochemical Impedance Spectroscopy Based Evaluation of Polypyrrole Electrochemically Deposited on the Pencil Graphite Electrode. *Colloids Surfaces A Physicochem. Eng. Asp.* **2021**, *610*, 125750. https://doi.org/10.1016/J.COLSURFA.2020.125750.

(74) Sharma, P. K.; Choudhury, D.; Karanwad, T.; Mohapatra, P.; Murty, U. S.; Banerjee, S. Curcumin Nanoparticles as a Multipurpose Additive to Achieve High-Fidelity SLA-3D Printing and Controlled Delivery. *Biomater. Adv.* **2023**, 213527. https://doi.org/10.1016/J.BIOADV.2023.213527.